Polymer 281 (2023) 126129

Contents lists available at ScienceDirect

Polymer

journal homepage: www.elsevier.com/locate/polymer

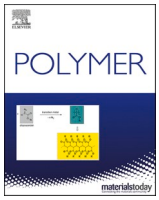

Synthesis and characterization of silk-poly(guluronate) hybrid polymers for the fabrication of dual crosslinked, mechanically dynamic hydrogels

Onur Hasturk, Jugal Kishore Sahoo, David L. Kaplan *

Tufts University, Department of Biomedical Engineering, Medford, MA, USA

ARTICLE INFO

Keywords:
Silk fibroin
poly(guluronate)
Biopolymer hydrogels
Dual crosslinking
Dynamic mechanics

ABSTRACT

The rapid ionic crosslinking of alginate has been actively studied for biomedical applications including hydrogel scaffolds for tissue engineering, injectable gels, and 3D bioprinting. However, the poor structural stability of ionic crosslinks under physiological conditions limits the widespread applications of these hydrogels. Moreover, the lack of cell adhesion to the material combined with the inability of proteases to degrade alginate further restrict utility as hydrogel scaffolds. Blends of alginate with silk fibroin have been proposed for improved structural and mechanical properties, but potential phase separation between the hydrophobic protein and the hydrophilic polysaccharide remains an issue. In this study, we demonstrated the synthesis of a hybrid biopolymer composed of a silk backbone with side chains of poly(guluronate) isolated from alginate to introduce rapid ionic crosslinking on enzymatically crosslinked silk-based hydrogels for on-demand and reversible stiffening and softening properties. Dual crosslinked macro- and microgels of silk fibroin-poly(guluronate) (SF-PG) hybrid polymers displayed dynamic morphology with reversible shrinking and swelling behavior. SF-PG hydrogel discs demonstrated dynamic mechanics with compressive moduli ranging from less than 5 kPa to over 80 kPa and underwent proteolytic degradation unlike covalently crosslinked alginate controls. SF-PG gels supplemented with gelatin substituted with tyramine or both tyramine and PG also supported the attachment and survival of murine fibroblasts, suggesting potential uses of these new hydrogels in mammalian cell culture to investigate cellular responses to dynamic mechanics or modeling of diseases defined by matrix mechanics, such as fibrosis and cancer.

1. Introduction

Hydrogels, which are defined as three dimensional networks of polymers with high water retention, tunable chemical composition and mechanical properties mimicking those of native tissues [1], have attracted attention in tissue engineering and regenerative medicine applications including for the 2D or 3D culture of cells [2], microencapsulation of multiple [3] or single cells [4,5], and injection-based delivery of drugs [6], growth factors [7], and cells [8,9]. Mechanically dynamic hydrogels with stimulus-responsive, on-demand stiffening/softening or degradation [10] have been of particular interest for a broad range of applications including for the study of cell mechanobiology [11,12] and stem cell differentiation [13], implantable gels for tissue regeneration [14], and modeling of fibrosis [15,16] or cancer [17,18]. Biomolecular hydrogels have several advantages over synthetic polymeric hydrogels, including lower toxicity and improved biocompatibility, and biodegradability [19]. In addition to protein-based hydrogels composed of collagen, gelatin, keratin, elastin, fibrin, silk fibroin or recombinant peptides [20]; the field of biomolecular hydrogels is largely dominated by polysaccharides derived from microorganisms, plants or animal origins, including cellulose, dextran, chitosan, hyaluronic acid, and particularly alginate [21] extracted from brown algae with high availability, low cost, and approval by the United States Food and Drug Administration (FDA) for applications in human [22]..

Alginate is a linear polysaccharide composed of 1,4-linked segments of (-D-mannuronic acid) (M) and (-L-guluronic acid) (G). Unlike the linear and flexible conformation of the M block segments, (1 → 4) linkages cause a steric hindrance around the carboxyl groups of G blocks, which results in a folded and rigid structural conformation and allows for rapid ionic crosslinking in the presence of divalent cations such as calcium or barium through a proposed mechanism called egg-box model [23]. Ionically crosslinked alginate hydrogels have been utilized in a wide range of regenerative medicine applications including injectable drug or cell delivery systems, cell encapsulating

* Corresponding author.
E-mail address: david.kaplan@tufts.edu (D.L. Kaplan).

https://doi.org/10.1016/j.polymer.2023.126129
Received 27 April 2023; Received in revised form 16 June 2023; Accepted 19 June 2023
Available online 20 June 2023

microspheres, and bioinks for 3D bioprinting [24]. Despite the rapid crosslinking and high gelling capacity, ionically crosslinked alginate hydrogels exhibit poor cell-matrix interactions due to the lack of cell recognition motifs [23], and limited structural stability because of the loss of ionic bridges by ion-exchange under physiological conditions [25]. Several strategies have been proposed to overcome these limitations, such as the covalent conjugation of cell adhesive arginine-glycine-aspartic acid (RGD) tripeptide on the alginate backbone to enhance cell adhesion [26], and the introduction of new crosslinking chemistries such as enzymatic [27] or photocrosslinking [28] via chemical modification of alginate to improve structural stability. Although these crosslinking strategies allowed for the fabrication of dual crosslinked hydrogels with dynamic mechanics through the on-demand formation of ionic bridges [27,29], the lack of enzymatic degradation by mammalian cells [30] required for remodeling of tissue scaffolds [31] remained an issue. Therefore, new strategies are needed to utilize the rapid ionic crosslinking of alginate without sacrificing bioactivity, structural stability, and to promote enzymatic degradation for biomedical applications.

Composites of alginate hydrogels with other biopolymers is a potential strategy to utilize ionic crosslinking for the fabrication of mechanically dynamic hydrogels. Blends of alginate with gelatin, for example, have been studied to take advantage of the thermal gelation and bioactivity through the intrinsic RGD peptides of gelatin for cell culture and 3D bioprinting applications [32]. The sol-gel transition of gelatin at physiological temperatures [33], however, renders these hydrogels structurally unstable. Another example of alginate composite hydrogels includes blends with silk fibroin (SF) [34], a biocompatible structural protein from the cocoons of *Bombyx mori* with extraordinary mechanical properties through self-assembly into crystalline β-sheets [35]. Mechanical properties and structural stability of ionically crosslinked silk/alginate blend hydrogels were further improved by physical crosslinking of the silk chains [36]. In addition to physical crosslinking, aqueous SF solutions can also be crosslinked covalently via dityrosine bond formation through horseradish peroxidase (HRP)/H_2O_2 [37] or tyrosinase activity [38], Fenton reaction [39], or photocrosslinking [40]. A potential limitation of SF/alginate blends, however, is the phase separation between the viscous, highly hydrophilic alginate and relatively hydrophobic silk, resulting in conformational changes in silk structure and inhomogeneity of the gels [34,41].

In this study, we propose the chemical modification of the SF backbone with poly(guluronic acid) (PG) blocks extracted from alginate to introduce ionic crosslinking and obtain dual crosslinked, mechanically dynamic gels, avoiding the phase separation between protein and polysaccharide phases that may impair the covalent crosslinking capacity of SF backbone. Extraction and ionic crosslinking of PG chains have been reported previously by others [42,43], but its conjugation on proteins to introduce ionic crosslinking has not been demonstrated before to our knowledge. Our results showed that PG chains were successfully conjugated on SF, significantly improving the solubility of lyophilized powders, and allowed for ionic crosslinking by Ca^{2+} ions without impairing dityrosine crosslinking of the SF backbone. Enzymatically crosslinked SF-PG gels displayed multiple cycles of stiffening by $CaCl_2$ and softening by sodium citrate treatments and underwent proteolytic degradation *in vitro* unlike alginate controls. Supplementing SF-PG gels with gelatin resulted in improved bioactivity without sacrificing the mechanically dynamic nature of the gels, implying potential applications in studying the influence of hydrogel stiffness on cell response such as fibrosis and stem cell fate.

2. Experimental

Extraction of PG from sodium alginate. Abbreviations for the side groups and the unmodified and modified polymers are listed in Table 1. PG chains were extracted from alginate (W201502, Sigma-Aldrich, St. Louis, MO) by partial acid hydrolysis (Fig. 1A) as described before [42].

Table 1
Descriptions of the frequently used abbreviations in the rest of the study.

Abbreviation	Description
PG	Poly(guluronate)
TA	Tyramine
G	Gelatin
G-TA	Tyramine-substituted gelatin
Alg	Alginate
Alg-TA	Tyramine-substituted alginate
SF	Silk fibroin
EDA	Ethylenediamine
SF-EDA	Ethylenediamine-substituted (aminated) silk fibroin
SF-PG	Poly(guluronate)-conjugated silk fibroin

Briefly, sodium alginate was dissolved in distilled water (dH_2O) at a concentration of 2% w/v under vigorous stirring overnight. Then 12 mL of 3 M HCl solution was added into 100 mL of alginate solution followed by refluxing for 5 h. After cooling to RT (24 °C) overnight, the solution was centrifuged at 9,000 rpm for 20 min and the supernatant was discarded. The pellet was resuspended in 130 mL dH_2O and stirred vigorously after adding 780 mg NaCl and ~770 μL of 10 M NaOH until a clear solution is obtained. The solution pH was adjusted to 2.25 with 12 M HCl and the solution was kept at RT for 2 h. The white precipitate was collected by centrifugation at 9,000 rpm for 20 min and resuspended in 25 mL dH_2O water. Next 80 mg of NaCl was mixed in and the solution pH was brought to 7.5 with 10 M NaOH, followed by the addition of 530 mg of activated carbon, and the solution was stirred for 2 h at RT. The activated carbon was removed by vacuum filtration and the PG chains were precipitated by addition of EtOH to a final concentration of 22% v/v. The product was precipitated overnight, collected by centrifugation at 9,000 rpm for 20 min, freeze dried, and stored at −20 °C until further use.

Gel Permeation Chromatography (GPC) analysis. GPC analysis was performed using a Waters Alliance 2695 GPC (Waters Corporation, MA) with a Waters Ultrahydrogel column. PEG and PEO standards were used for comparison. 0.1 M sodium nitrate was used as the mobile phase. The chromatograms were analyzed using the Empower 3.0 GPC software (Waters Corporation, MA).

Synthesis of tyramine-conjugated gelatin (G-TA) and alginate (Alg-TA). Tyramine-substituted gelatin (G-TA) (Fig. 1B) and alginate (Alg-TA) (Fig. 1C) were synthesized through carbodiimide coupling reaction. Briefly, 2% w/v solutions of gelatin type A from porcine skin (G2625, gel strength ~175 g Bloom, Sigma-Aldrich, St. Louis, MO) or sodium alginate were prepared in 0.05 M MES buffer (pH 6.0) and reacted with tyramine hydrochloride (Sigma-Aldrich, St. Louis, MO) (500 mg per 1 g protein) in the presence of EDC (184 mg per 1 g protein) and NHS (57 mg per 1 g protein) under stirring at room temperature (24 °C) for 18 h. The solution was dialyzed against distilled water using 3.5 MWCO tubing at 37 °C with 6 changes over 3 days. The dialyzed solution was frozen overnight at −80 °C overnight, lyophilized and stored at −20 °C until further use.

Extraction and amination of SF. Five g of cut cocoons were boiled in 2 L of 0.02 M sodium carbonate solution for 30, 60 or 120 min to remove sericin. Degummed fibers were rinsed 3 times with dH_2O and dried overnight. Dry fibers were solubilized in 9.3 M LiBr solution at a concentration of 20% w/v for 3 h at 60 °C and cooled down to RT. Amination was performed by carbodiimide coupling of ethylenediamine (EDA) (Fig. 1D–i). SF in LiBr solution was diluted to 2% w/v in 0.05 M (2-(N-morpholino)ethanesulfonic acid) MES buffer (pH 6.0). 0.5 g of EDA dihydrochloride, 180 mg of 1-Ethyl-3-(3-dimethylaminopropyl) carbodiimide hydrochloride (EDC) and 60 mg of N-hydroxysuccinimide (NHS) (Sigma-Aldrich, St. Louis, MO) were added per 1 g of SF, and the solution was stirred for 18 h at RT under gentle stirring. The reaction mixture was dialyzed against dH_2O in 3.5 kDa cutoff tubing for 5 days with 10 water changes and concentrated to ~4% w/v by water evaporation in a fume hood. Insoluble particles were removed by

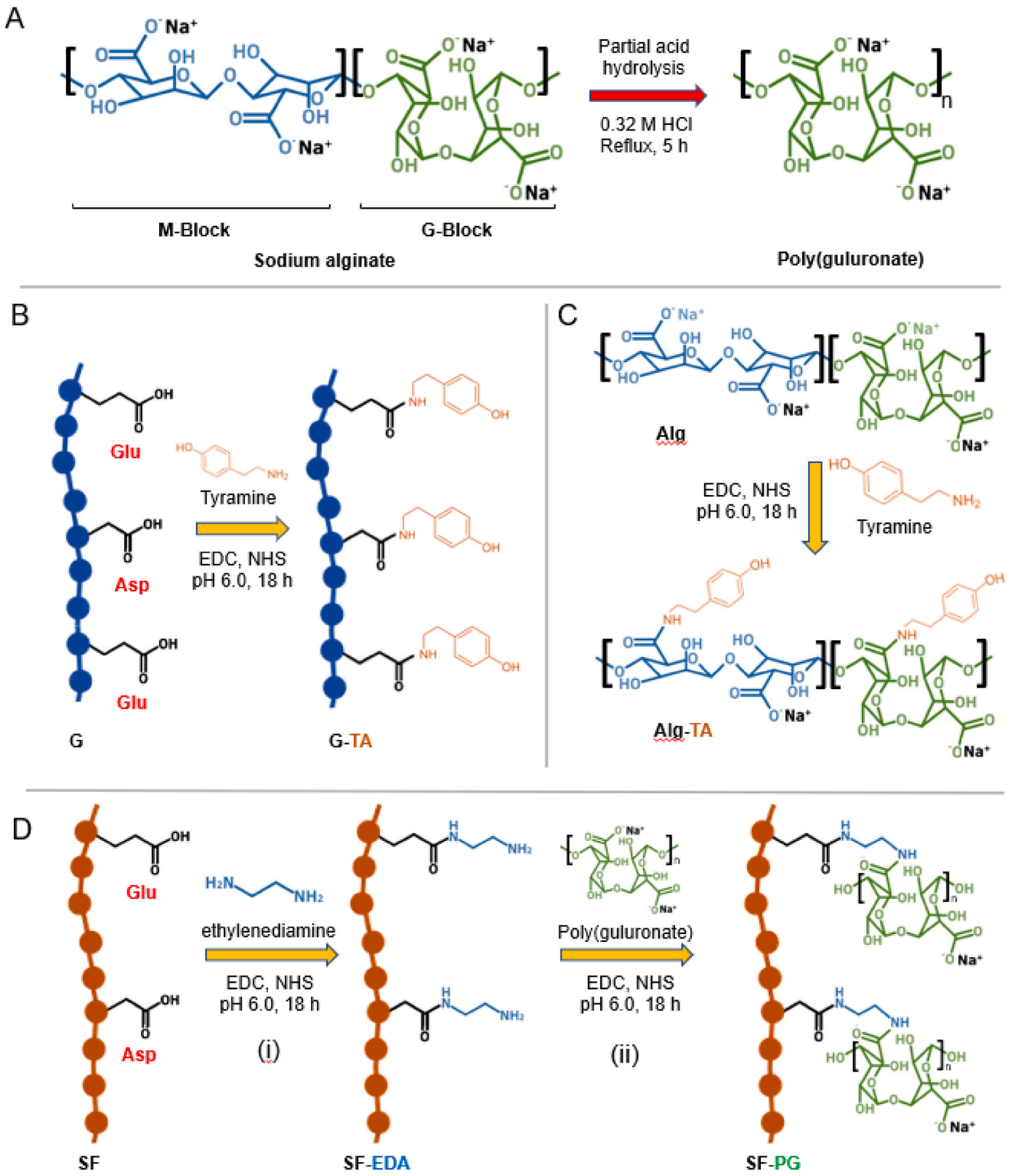

Fig. 1. Schematic representation of the chemical modification of gelatin, alginate, and silk fibroin (SF). (**A**) Extraction of poly(guluronate) (PG) chains from the G-blocks of sodium alginate by partial acid hydrolysis. Carbodiimide coupling of tyramine (TA) on (**B**) gelatin (G) and (**C**) alginate (Alg) for the synthesis of tyramine-substituted gelatin (G-TA) and alginate (Alg-TA), respectively. (**D**) Synthesis of silk fibroin-poly(guluronate) (SF-PG) through (**i**) carbodiimide coupling of ethylenediamine (EDA) residues on the carboxylic acid moieties of aspartic and glutamic acids on silk fibroin (SF) followed by (**ii**) carbodiimide coupling of PG chains on primary amine residues of SF-EDA.

centrifugation at 9,000 rpm for 20 min at 4 °C, and the SF-EDA solution was stored at 4 °C.

Synthesis and characterization of SF-PG. SF-PG was synthesized by carbodiimide coupling of PG chains on aminated SF (SF-EDA) (Fig. 1D–ii). 2% w/v of SF-EDA solution was prepared in 0.05 M MES buffer (pH 6.0) and mixed with 1 g of PG powder per 1 g protein. 180 mg of EDC and 60 mg of NHS were added per 1 g of protein, and the reaction mixture was stirred for 18 h at RT and dialyzed against dH_2O in 20 kDa cutoff tubing for 5 days with 10 water changes. The dialyzed solutions were centrifuged at 9,000 rpm for 20 min at 4 °C to remove insoluble particles, freeze dried, and stored at −20 °C. Using the same approach, gelatin type A (G) with or without tyramine (TA) modification was conjugated with PG chains to obtain G-PG and G-TA-PG constructs. For ^1H NMR, lyophilized PG, SF and SF-PG powder was dissolved in deuterated water (D_2O) at a concentration of 10 mg/mL and analyzed using a 500 MHz Bruker Avance III NMR spectrometer. SF-PG synthesized using 30-, 60- or 120 min-degummed SF, G-PG and G-TA-PG were dissolved in dH_2O at a concentration of 1 mg/mL, and UV absorbance at 280 nm was measured using a SpectraMax M2 multi-mode microplate reader (Molecular Devices, Sunnyvale, CA). The weight% of protein backbone was quantified using the calibration curves plotted using OD280 values of SF-EDA, gelatin, or G-TA solutions with a concentration in the range of 0.1–1 mg/mL.

Fabrication of dual crosslinked hydrogels. SF-PG powders synthesized using 60- or 120-min degummed SF were dissolved in dH_2O at 7.5% w/v and supplemented with 100 U/mL HRP. Gelation was induced by adding H_2O_2 to a final concentration of 0.03% v/v, and hydrogel discs were fabricated by incubation of 200 μL solution at 37 °C for 1 h in cylindrical polydimethylsiloxane (PDMS) molds with a diameter of 8 mm. After the completion of gelation, ionic crosslinking of PG side chains was induced by incubation of hydrogel samples in 20 mM $CaCl_2$ for 24 h. On-demand cleavage of the ionic bridges was achieved by incubating the dual crosslinked hydrogels in 20 mM solution of sodium citrate as the calcium chelator for 24 h. Alternatively, 3.5% w/v SF-PG/G-TA (6:1 w/w), 5% w/v G-TA-PG, or 5% w/v G-TA-PG/SF-PG (1:1 w/w) were supplemented with 10 U/mL of HRP and the gelation was induced in PDMS molds by adding H_2O_2 to a final concentration of 0.01% v/v. Formation and cleavage of ionic bridges was performed by incubation with 20 mM $CaCl_2$ or sodium citrate, respectively.

Fabrication of Alg-TA/SF-PG hydrogel microbeads. A blend of 2% w/v Alg-TA and 6% w/v SF-PG in 40 mM 4-(2-hydroxyethyl)-1-piperazineethanesulfonic acid (HEPES) with 5% w/v dextrose (HD) solution (pH 7.4) was used as the pre-hydrogel solution for the fabrication of hydrogel microbeads by centrifugation-based droplet formation as described before [44]. Briefly, 20 μL of pre-hydrogel solution supplemented with 100 U/mL of HRP was loaded into a 34G needle (inner diameter of 51 μm) and extruded into the crosslinking buffer (40 mM HEPES, 5% w/v dextrose, 20 mM $CaCl_2$ and 0.5 mM H_2O_2) by centrifugation at 2,250 g for 1 min using an Eppendorf 5804 R centrifuge with a T-60-11 horizontal rotor. Hydrogel microbeads collected in the bottom of the tube were resuspended by pipetting, incubated at 37 °C for 30 min, collected by centrifugation at 2,250 g for 1 min, and resuspended in fresh HD buffer with or without 20 mM sodium citrate. Microbeads treated with sodium citrate were washed three times with HD buffer and resuspended in HD buffer supplemented with 20 mM $CaCl_2$ to reform the ionic bridges. The morphology of the microbeads was monitored by phase contrast imaging of using a BZ-X700 Fluorescence Microscope (Keyence Corp., Itasca, IL). Diameters of the microbeads were quantified on the phase contrast micrographs using the image analysis software ImageJ (1.48v, NIH, USA).

Unconfined compression test of hydrogels. Compression test was performed (n = 5) using a RSA3 Dynamic Mechanical Analyzer (TA Instruments, New Castle, DE, USA) between 10 mm stainless steel parallel plates. Hydrogel discs were exposed to a preload of ~0.5 g to ensure full surface contact. An initial cycle of loading and unloading was performed at 30% strain at a rate of 1% s^{-1} to eliminate artifacts, and the stress-strain response and elastic recovery were monitored during the second cycle at the same strain rate. Compressive moduli were calculated by the tangent modulus of the loading phase from 0 to 5% strain.

Water content and *in vitro* enzymatic degradation. Hydrogel discs prepared from 200 μL solutions in PDMS molds were incubated in phosphate buffered saline (PBS) at room temperature for 4 h. One set of hydrogels were weighed and then lyophilized to determine water content. Another set of hydrogels were transferred into 300 μL of 0.001 U/mL of α-chymotrypsin from bovine pancreas (Sigma-Aldrich, St. Louis, MO) dissolved in PBS and incubated for 1, 3, or 8 days. The enzyme solution was changed every 2 days. After removal of enzyme solution, hydrogels were washed in Ultrapure™ distilled water (ThermoFisher Scientific, Waltham, MA) over night at RT, lyophilized and weighed. Results are reported as the mass fraction of the initial weight at day 0 (n = 5).

Cell Culture. L929 fibroblasts from mouse subcutaneous connective tissues (ATCC, Manassas, VA, USA) were cultured in high-glucose Dulbecco's Modified Eagle's Medium (DMEM) supplemented with 1% antibiotic-antimycotic, and 10% fetal bovine serum (FBS) (ThermoFisher Scientific, Waltham, MA, USA). Cells seeded in 48-well plates at a density of 8000 cells/cm^2 were cultured for 24 h at 37 °C with 5% CO_2, and the growth medium was replaced with medium supplemented with 5–30 mM $CaCl_2$. After 1 and 8 days of culture, cell viability was assessed by Live/Dead staining kit (Invitrogen, Carlsbad, CA) according to manufacturer instructions and imaging using the fluorescence microscope to determine the impact of $CaCl_2$ concentration on cell viability and growth.

Pre-hydrogel solutions were sterile filtered using 0.22 μm syringe filters and 200 μL solution was enzymatically crosslinked in autoclaved PDMS molds. Hydrogel discs were transferred into 24-well plates and L929 fibroblasts suspended in 50 μL of culture medium were seeded on hydrogel surface at a density of 8,000 cells/cm^2. After 2 h for cell attachment, culture medium was added to each well. After incubation for 24 h, culture medium was replaced with fresh medium supplemented with 20 mM $CaCl_2$ and the samples were cultured for 24 h to achieve ionic crosslinking. Samples were rinsed with PBS three times and incubated in fresh culture medium supplemented with 20 mM sodium citrate for 24 h to cleave ionic bridges. Cell viability was assessed by with Live/Dead staining.

Statistical analysis. All data are expressed as mean ± standard deviation for $n \geq 3$. GraphPad Prism (GraphPad Software, La Jolla, CA) was used to perform One- or Two-way analysis of variance (ANOVA) with Tukey's post hoc multiple comparison test to determine statistical significance ($^*p \leq 0.05$, $^{**}p \leq 0.01$, $^{***}p \leq 0.001$).

3. Results and discussion

Hydrogels of biopolymers with dynamic and reversible mechanical properties hold great promise as scaffold materials to model *ex vivo* tissues for understanding the mechanisms of cell response and fate, tissue organization and remodeling, and disease progression including cancer and fibrosis as well as development of therapeutic approaches. Physical and enzymatic crosslinking of silk combined with reversible ionic crosslinking of alginate is an excellent candidate for the fabrication of composite hydrogels with robust and dynamic mechanics. Problems emerging from the phase separations and conformational changes in silk structure within aqueous blends of hydrophobic silk and highly viscous and hydrophilic alginate, however, significantly limit potential applications of silk/alginate composite gels. The aims of this study included: (a) developing a novel hydrogel formulation combining robust mechanics, structural stability, enzymatic crosslinking, and proteolytic degradability of silk backbone with, (b) the high solubility and rapid ionic crosslinking of alginate as an alternative to ionically crosslinked alginate gels with poor stability under physiological conditions [25], covalently crosslinked alginate gels lacking proteolytic degradation [30], or potential phase separations with hydrophobic polymers such as

silk [41]. To achieve these goals, here we developed a novel hybrid polymer composed of a silk fibroin (SF) backbone with covalently conjugated branches of poly(guluronate) (PG) oligosaccharide chains extracted from alginate, combining enzymatic crosslinking of silk and ionic crosslinking of PG for the fabrication of dual crosslinked, on-demand stiffening and softening hydrogels. The advantages of our SF-PG polymer over traditional silk/alginate blends include improved water solubility of silk backbone through high hydrophilicity of PG branches which allows for dry storage and significantly longer shelf life, no phase separations between the protein and polysaccharide components in aqueous solutions, and most importantly, preservation of the enzymatic crosslinking of silk backbone allowing for the fabrication of dual crosslinked gels with reversible, dynamic mechanics. Moreover, the proposed strategy is not limited to silk and can be applied to practically any protein, allowing for combinations of the unique properties of proteins with the rapid ionic crosslinking of alginate.

Guluronic acid units in the oligosaccharide chains extracted from alginate by partial acid hydrolysis carry a carboxylic acid moiety, allowing for its conjugation on primary amine residues such as the lysine side chains on proteins through carbodiimide coupling. Since the lysine content of silk fibroin heavy chain is low (0.2 mol%) [45], the initial step for the conjugation of PG chains on silk was to convert carboxylic acid side chains on aspartic (0.5 mol%) and glutamic acid (0.6 mol%) [45] into primary amines through carbodiimide coupling of EDA as we reported before for the synthesis of aminated silk [46]. GPC analysis revealed that the number and weight average molecular weights of the PG chains extracted from alginate by 5h of acid reflux as Mn = 6169 and Mw = 8021, respectively (Supplementary Fig. S1), which was parallel with the previous reports of ~6 kDa [42]. After the carbodiimide coupling, the reaction mixture was dialyzed using 20 kDa cutoff dialysis tubing to ensure removal of unconjugated excess PG. The chemical nature of SF-PG was compared to those of PG and unmodified SF by ^{1}H NMR spectroscopy. The peaks at ~4.9, 4.3, 3.9, 3.8 and 3.7 ppm in the NMR spectrum of PG (Fig. 2A) reflect the G_1, G_5, G_4, G_3 and G_2 protons of guluronate monomer, respectively, as reported before [47]. Significantly smaller peaks at ~4.5, 3.6 and 3.5 ppm assigned to M_1, M_3 and M_5 protons of mannuronate, respectively, indicated that the acid hydrolysate of alginate was primarily composed of PG domains. In addition to proton peaks from regenerated silk (Fig. 2B), the NMR spectrum of SF-PG (Fig. 2C) also displayed a clear peak at at ~2.7 ppm originating from the EDA protons and the G1, G5 and G4 peaks of PG chains, implying the successful conjugation of PG chains on aminated SF. G3 and G2 peaks of PG chains could also be seen overlapping with Gly $C^{\alpha}H_2$ and Ser $C^{\beta}H_2$ peaks at 3.2–3.8 ppm from the SF backbone.

The silk backbone and PG side chain contents of SF-PG were determined by UV–Vis spectroscopy by taking advantage of the high UV absorption by silk through tyrosine side chains at 280 nm[48] unlike PG chains. Using the calibration curves plotted by OD_{280} vs known concentrations of aminated silk (Fig. 3A–i), the weight% of SF backbone within the SF-PG hybrid was quantified for different degumming times (Fig. 3A–ii). A decrease was recorded in the weight ratio of PG chains in SF-PG from 77% to 71% and 69% with increasing degumming time from 30 to 60 and 120 min, respectively. This could be attributed to protein hydrolysis during degumming, particularly at the light chain and the c-termini and the hydrophilic spacer domains of heavy chain [49] where lysine, aspartic acid and glutamic acids are located [48], likely resulting in loss of some potential PG conjugation sites during dialysis after degumming. More than 60% of the SF-PG weight being composed of PG indicated a SF structure highly branched with PG chains. Freezing and lyophilization are known to induce crystallization of the random coils of hydrophobic silk domains into β-sheets, significantly decreasing the solubility of regenerated SF [50,51]. Lyophilized powders of SF-PG (Fig. 3B–i) synthesized using 120- or 60-min degummed SF dissolved rapidly in dH_2O at a concentration of 8% w/v and formed a non-viscous solution (Fig. 3B–ii), suggesting a significant increase in water solubility of lyophilized SF upon conjugation of PG chains. Moreover, no phase separation was observed within the solution after 24 h of incubation at 4 °C, implying an important benefit over silk/alginate blends. Despite having the highest PG weight%, SF-PG synthesized using 30 min degummed SF was only partially soluble at this concentration likely due to higher molecular weight and crystallinity of the SF backbone at lower degumming times [52]. Better solubility of SF-PG over unmodified SF allowed for dry storage as lyophilized powder at −20 °C more than a year, significantly improving the shelf-life compared to the significantly

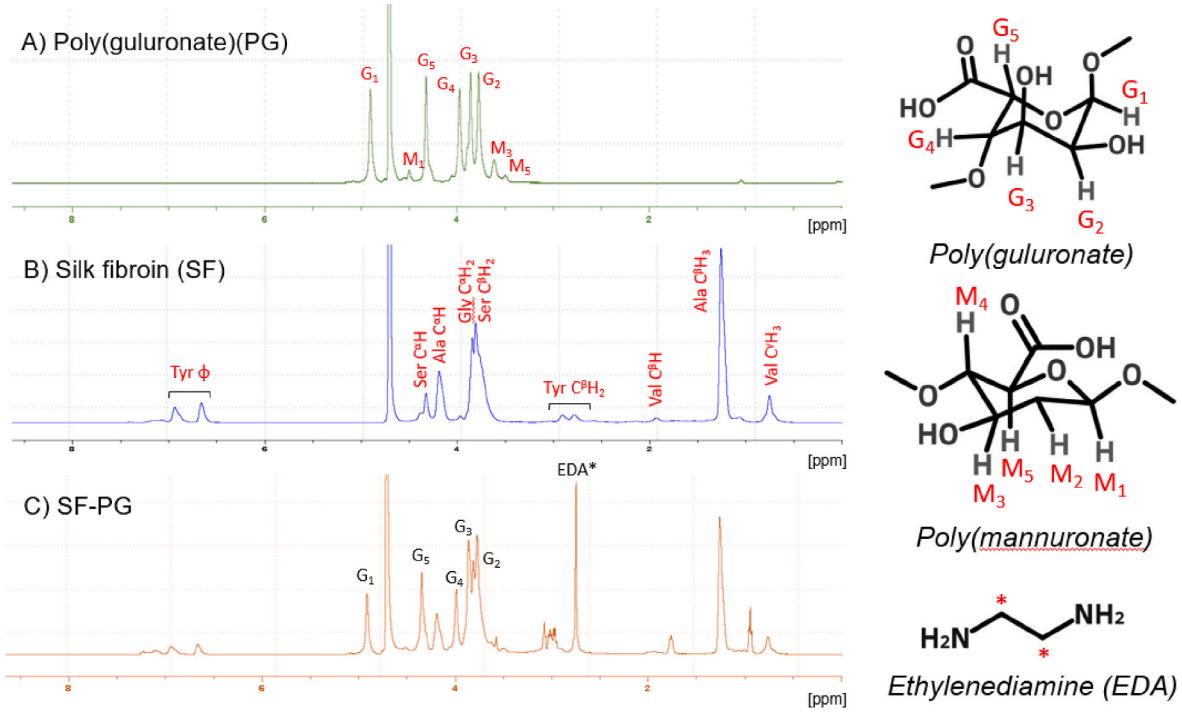

Fig. 2. ^{1}HNMR spectra of (A) poly(guluronate) (PG), (B) silk fibroin (SF), and (C) silk-poly(guluronate) hybrid (SF-PG).

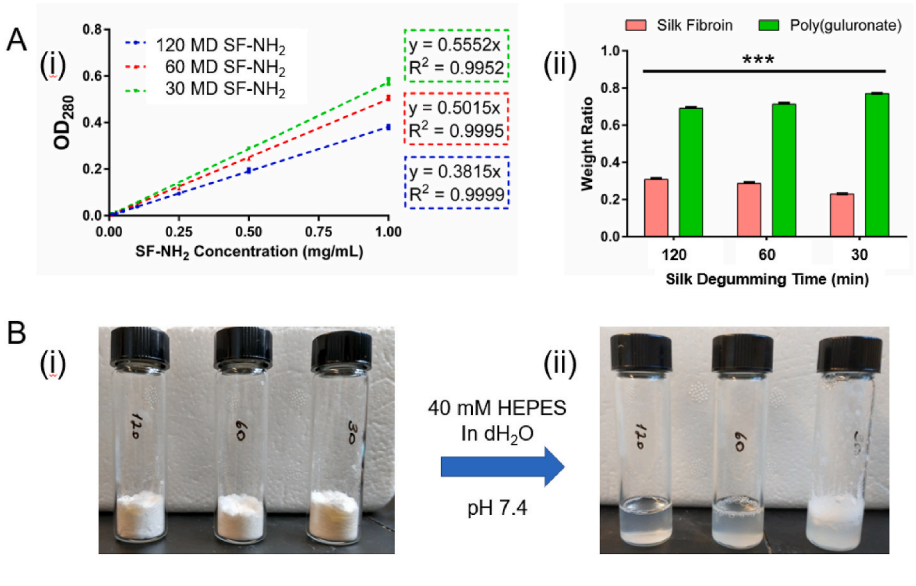

Fig. 3. Composition and solubility of SF-PG synthesized using silk extracted at different degumming times. (A) (i) Standard curves of UV absorption (280 nm) versus concentration of 120, 60 or 30 min degummed (MD) aminated silks. (ii) Weight ratios of silk and poly(guluronate) in SF-PG quantified from OD_{280} of silk backbone (n = 5, *p < 0.05, **p < 0.01 and ***p < 0.001). (B) Solubility of (i) lyophilized SF-PG powders prepared using 120-, 60- or 30-min degummed silk in (ii) 40 mM HEPES in dH_2O after 1 h of stirring at room temperature.

shorter storage of SF solution at 4 °C due to spontaneous gelation [53].

Aqueous solutions of the SF-PG hybrid synthesized using 60- or 120-min degumming were used for the fabrication of dual crosslinked hydrogels through HRP-mediated dityrosine crosslinking of SF backbone followed by the ionic crosslinking of PG chains with Ca^{2+} ions (Fig. 4A). Considering potential impacts of calcium ions on cell viability [54], metabolism and proliferation [55], $CaCl_2$ concentration was first optimized by monitoring the viability of murine fibroblasts cultured with $CaCl_2$ containing medium for 8 days. Live/dead assay at days 1 and 8 showed no significant difference within the range of 5–30 mM $CaCl_2$ (Fig. S2), so 20 mM $CaCl_2$ was used for the formation of ionic bridges for the rest of the study. Enzymatic crosslinking of SF-PG resulted in highly elastic, transparent hydrogels, and the 8% w/v SF-PG hydrogel fabricated using 60 min degummed (MD) silk had a water content of ~93% (Fig. S3), resulting in a polymer to water ratio of ~0.053. SF-PG gels shrank significantly and became opaque upon incubation in $CaCl_2$, and

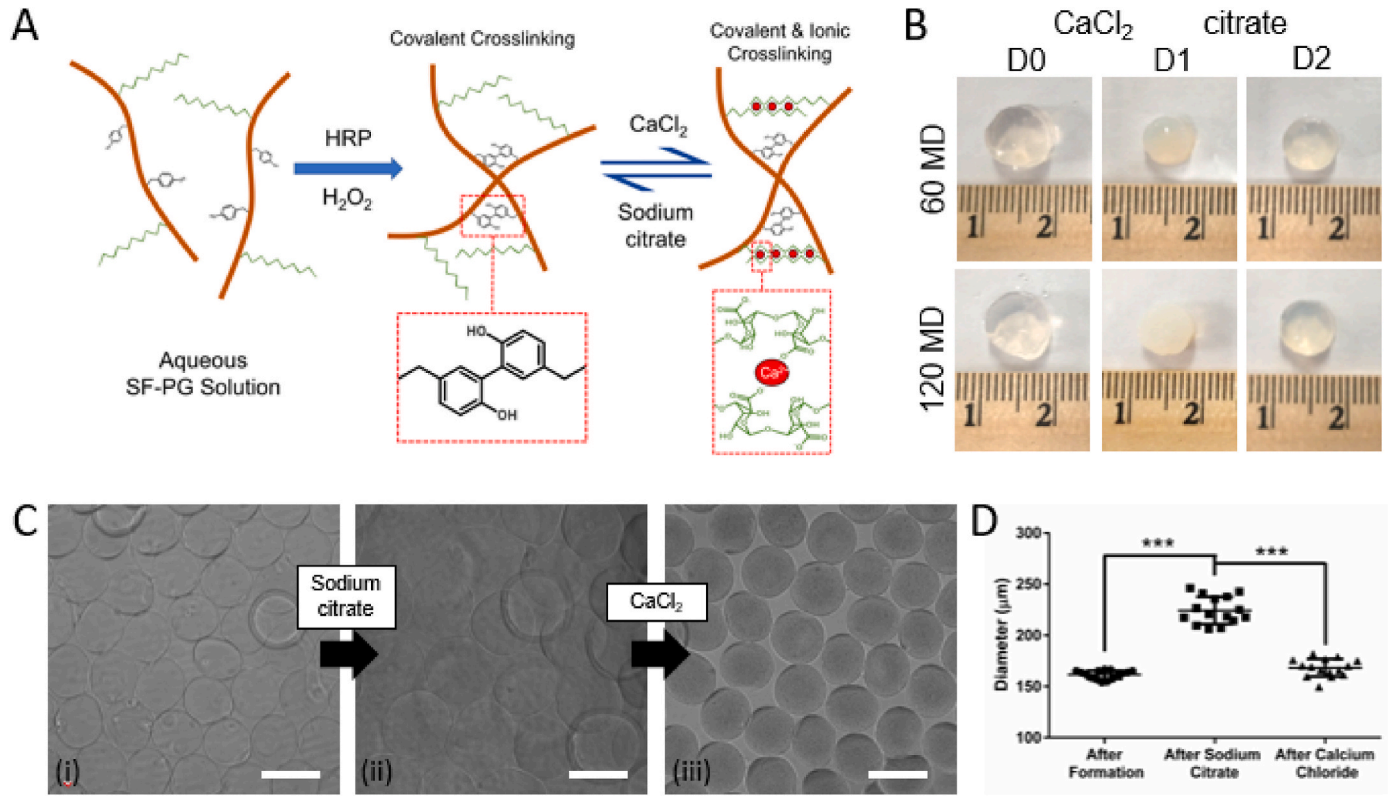

Fig. 4. Fabrication and morphology of dual crosslinked SF-PG hydrogels and Alg-TA/SF-PG microgel beads. (A) Schematic illustration of enzymatic dityrosine crosslinking of aqueous SF-PG solution by HRP/H_2O_2 activity followed by reversible formation and cleavage of ionic crosslinks by $CaCl_2$ and sodium citrate treatments, respectively. (B) Morphology of SF-PG hydrogels (using 60 or 120 min degummed (MD) silk fibroin) after treatment with $CaCl_2$ and sodium citrate. (C) Morphology and (D) diameter of Alg-TA/SF-PG microgel beads in response to sodium citrate treatment followed by CaCl2 for cleavage and reformation, respectively, of ionic bridges between PG side chains. (n = 15, *p < 0.05, **p < 0.01 and ***p < 0.001).

expanded and became transparent again upon incubation with sodium citrate (Fig. 4B), indicating the formation and cleavage of ionic bridges, respectively, between the PG chains. Enzymatic crosslinking of SF-PG is an important advantage over the blends of SF with alginate, which we previously demonstrated to fail to undergo enzymatic crosslinking [44] likely due to phase separation and conformational changes in silk at high concentrations of alginate, resulting in reduced accessibility of the tyrosine side chains.

In addition to macroscale gels, we also employed SF-PG for the fabrication of dual crosslinked hydrogel microbeads by the centrifugation-based droplet formation strategy. SF-PG solution was supplemented with Alg-TA to provide high viscosity required for flow mechanics to form individual droplets in quasi-static dripping regime [56] as well as enhancing the gelation kinetics through crosslinking of tyramine moieties on alginate with tyrosine side chains on SF-PG. Centrifugation of Alg-TA/SF-PG solution through 34-gauge needles into a dual crosslinking bath with $CaCl_2$ and H_2O_2 resulted in fabrication of hydrogel microbeads (Fig. 4C–i) with an average diameter of ~160 μm (Fig. 4D). Upon incubation with sodium citrate, the microbeads swelled (Fig. 4C–ii) and the average diameter rose to ~220 μm (Fig. 4D), indicating cleavage of ionic bridges through chelation of calcium ions. Microgels shrank (Fig. 4C–iii) back to their original size (Fig. 4D) after incubation with calcium ions, implying reversibility of ionic bridges on demand to modulate the dimensions of hydrogels also in microscale.

Mechanical testing of the SF-PG hydrogel discs revealed on demand stiffening and softening by treatment with $CaCl_2$ or sodium citrate, respectively, accompanied by a reversible change in elasticity manifested by a significant increase and decrease, respectively, in the hysteresis shown in the stress-strain curves in Fig. 5A–i and **5A-ii**. Initial compressive moduli of the enzymatically crosslinked 7.5% w/v SF-PG hydrogels for 60 min and 120 min degumming were ~2 and ~1.4 kPa, respectively, which increased more than 13-fold to ~27 kPa upon ionic crosslinking in $CaCl_2$ bath (Fig. 5A–iii), and then dropped to ~5.4 and ~3.1 kPa, respectively, upon cleavage of ionic crosslinks by sodium citrate treatment (Fig. 5A–iii). The difference between initial and post-citrate compressive moduli of SF-PG gels could be explained with the physical crosslinking of SF-backbone through self-assembly into crystalline β-sheets during incubation with $CaCl_2$ and sodium citrate solutions with relatively higher ionic strength. This was more evident when 120 MB SF-PG hydrogels were treated with $CaCl_2$ and sodium citrate in cycles for 96 h, causing a cyclic change in the elasticity (Fig. 5B–i) and stiffness (Fig. 5B–ii) with a gradual increase in compressive modulus from 1.4 to ~ 6.6 kPa at only-enzymatically crosslinked state. It should also be noted that upon incubation with $CaCl_2$ for 3 days from days 4–7 increased compressive modulus to ~87 kPa (Fig. 5B–ii), indicating control over the extent of ionic crosslinking and resulting stiffness by altering the incubation time with calcium ions.

Cellular response to SF-PG hydrogels was tested by 2D culture of murine fibroblasts on 8% w/v gels. Live/dead micrographs (Fig. 6A) revealed that a large proportion of the cells were dead 24 h after seeding on SF-PG hydrogel, suggesting poor cell-matrix interactions. This could be attributed to the lack of cell adhesion sequences in both SF [57] and alginate [58] as well as the high hydrophilicity of PG chains that likely impacted the absorption profile of proteins from the serum in culture media [59]. To overcome this limitation, SF-PG was blended with G-TA to incorporate the intrinsic cell adhesive RGD sequences of gelatin backbone [60] into the enzymatically crosslinked polymer network. Indeed, a small weight ratio of G-TA not only improved cell viability on

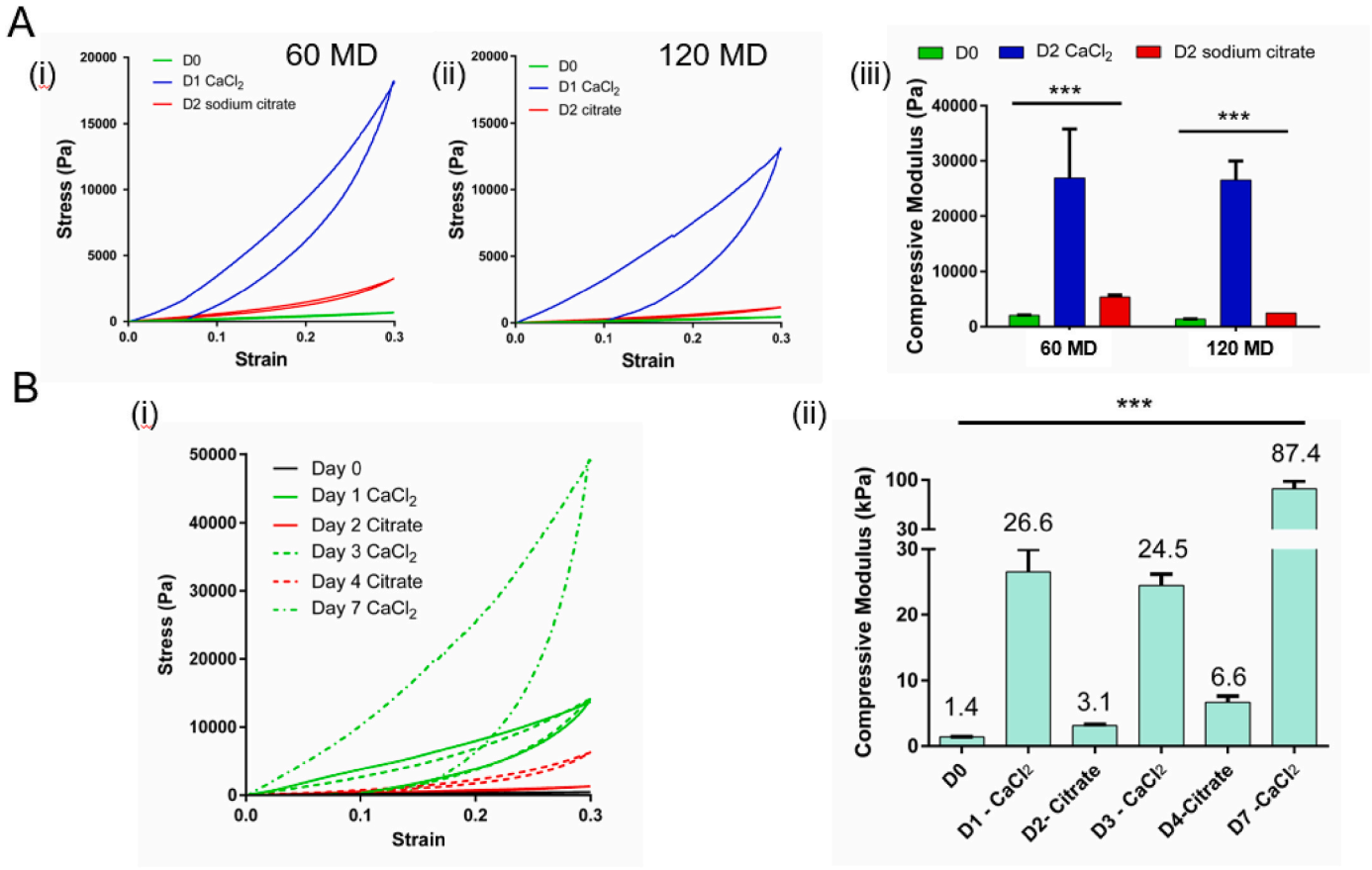

Fig. 5. Compressive mechanical properties of SF-PG hydrogels. (A) Stress-strain curves (i, ii) and compressive moduli (iii) of 7.5% w/v SF-PG (using 60 or 120 min degummed (MD) silk fibroin) hydrogels on days 0, 1 and 2 after enzymatic crosslinking, 24 h of incubation with $CaCl_2$, and 24 h of incubation with sodium citrate, respectively. (B) Stress-strain response (i) and compressive moduli (ii) of 120 MB SF-PG gels upon cyclic stiffening and softening by $CaCl_2$ and sodium citrate treatments, respectively, over 7 days (n = 5, *p < 0.05, **p < 0.01 and ***p < 0.001).

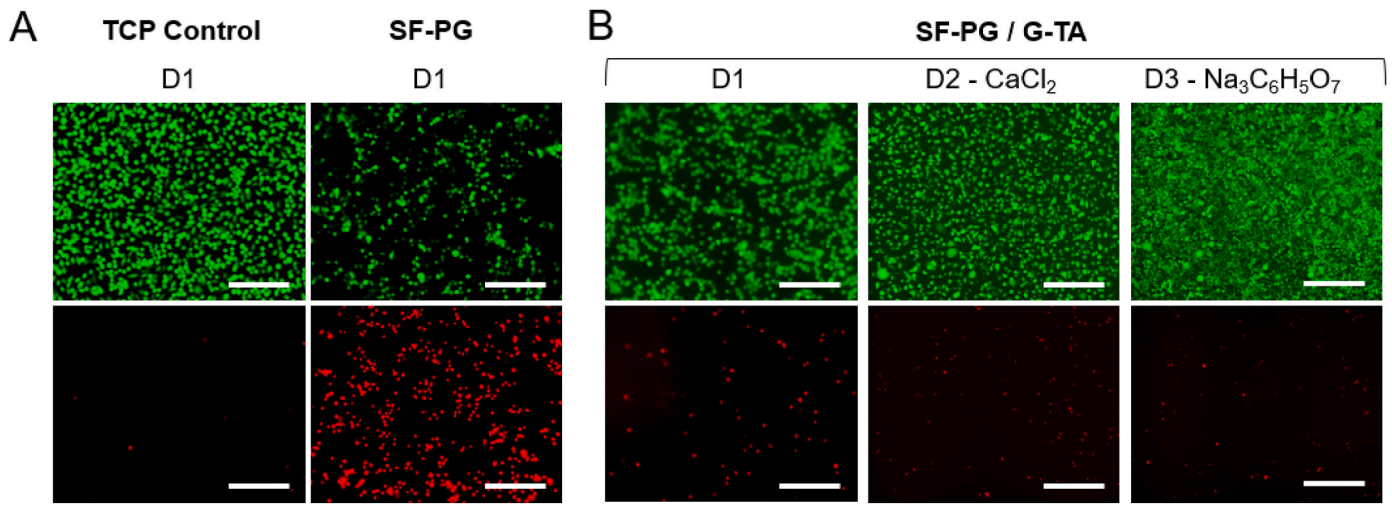

Fig. 6. Live dead micrographs of L929 fibroblasts cultured on (A) TCP control, 8% w/v SF-PG or (B) 3% w/v SF-PG/0.5% G-TA composite hydrogels. Formation and cleavage of ionic bridges within SF-PG/G-TA composite gels were induced by 24 h incubation of samples with 20 mM calcium chloride ($CaCl_2$) and sodium citrate ($Na_3C_6H_5O_7$), respectively, to monitor impact on cell viability. Green: calcein (live), red: EthD-1 (dead), scale bars: 200 μm. (For interpretation of the references to colour in this figure legend, the reader is referred to the Web version of this article.)

SF-PG hydrogels at day 1 significantly (Fig. 6B), but the high availability of phenol side chains on G-TA for enzymatic crosslinking [57] also allowed for lower total polymer, HRP and H_2O_2 concentrations required to obtain a structurally stable hydrogels. SF-PG/G-TA gels had a higher water content at around 95% (Fig. S3) than 8% SF-PG gels as expected because of lower total polymer concentration. Treatments with $CaCl_2$ from day 1–2 and sodium citrate from day 2 to day 3 for hydrogel stiffening and softening, respectively, did not cause any significant impact on cell viability and the cells were able to proliferate (Fig. 6B). Like SF-PG only gels, SF-PG/G-TA gels also displayed opacification upon incubation in $CaCl_2$ bath (Fig. 7A) accompanied with an increase in hysteresis in the stress-strain curve (Fig. 7B) and a ~2.5-fold increase in compressive modulus (Fig. 7C), which were reversed after treatment with sodium citrate. We speculate that highly bioactive hydrogels with dynamic mechanics within a wide range of initial and final stiffness values could be fabricated by altering the total polymer concentration and the weight ratios of SF-PG and G-TA.

Enzymatic degradation of scaffold materials at a controllable rate is a key factor in tissue engineering and regeneration for the formation and remodeling of new tissue [61]. The polysaccharide alginate can be hydrolyzed by the enzyme alginate lyase (alginase), which is produced by some bacteria, fungi and algae but not by animal cells [62]. Thus, covalently crosslinked alginate hydrogels cannot be remodeled actively by the cells but instead degrade slowly through loss of ionic crosslinks in body fluids [28]. SF, on the other hand, can undergo proteolytic degradation at controllable rates compared to other rapidly degrading proteins such as gelatin or collagen thanks to the high crystallinity of hydrophobic domains, providing structural support for cellular organization for a sufficient time until complete breakdown without hindering longer-term matrix remodeling [63]. Enzymatically crosslinked Alg-TA gels as a control and SF-PG and SF-PG/G-TA gels as novel formulations were incubated with the protease chymotrypsin for 8 days to assess their proteolytic degradability. The percent weight of hydrogel discs remaining after 1, 3 or 8 days of incubation with protease (Fig. 7D)

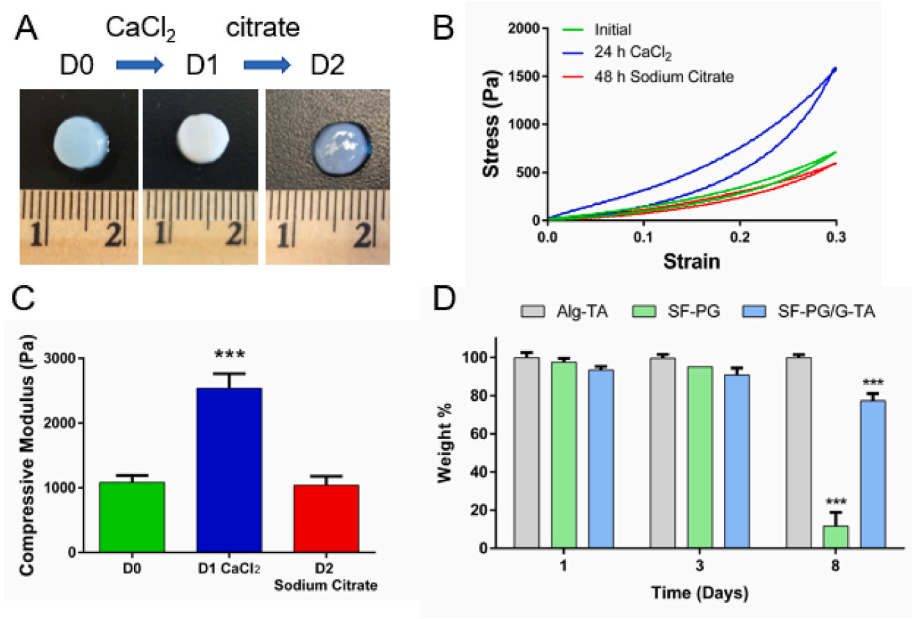

Fig. 7. Characterization of SF-PG and SF-PG/G-TA hydrogels. (A) Morphologies, (B) stress-strain responses and (C) compressive moduli (n = 5) of 3% w/v SF-PG/0.5% G-TA composite hydrogels at day 0 after fabrication, at day 1 after 24 h of incubation in $CaCl_2$, and at day 2 after 24 h of incubation in sodium citrate solution. (D) *In vitro* enzymatic degradation (n = 4) of Alg-TA, SF-PG and SF-PG/G-TA hydrogels quantified by % weight remained compared to day 0 after incubation with 0.001 U/mL solution of α-chymotrypsin in PBS. (*$p < 0.05$, **$p < 0.01$ and ***$p < 0.001$; asterisks above the bars represent statistical significance compared to day 1 samples).

showed that unlike Alg-TA gels, both SF-PG and SF-PG/G-TA composite gels lost mass through proteolytic degradation. Interestingly, degradation of 8% w/v SF-PG gels was faster compared to 3% w/v SF-PG/0.5% w/v G-TA gels, the former having less than 20% of its initial weight left while more than 70% of the latter remained after 8 days of incubation. This could be explained with higher crosslinking density in the presence of G-TA as we also demonstrated previously with SF/G-TA gels compared to SF-only controls [57].

Inspired by the impact of G-TA on bioactivity of SF-PG gels, we expanded the PG modification strategy to gelatin. Unmodified and tyramine-substituted gelatin type A from porcine skin was carbodiimide coupled with PG chains (Fig. S4A) without any pre-treatment because of its sufficient number of lysines (2.7 mol% [64]). UV spectroscopic analysis of protein backbone content quantified using the calibration curves with OD_{280} (Fig. S4B) revealed a PG content of ~33% and 50% for G-PG and G-TA-PG, respectively, which was lower than those of SF-PG (69–77%). This could be attributed to the isoelectric point of gelatin type A from porcine skin being within the alkaline range (pH 7–9.4) [65], resulting in a net negative charge on the protein backbone and likely limiting gelatin and PG chains coming in close proximity during carbodiimide coupling due to electrostatic repulsion. Thus, G-TA-PG having a larger PG content could be explained with some of the carboxylic acid residues being occupied by tyramine moieties [57], lowering the net negative charge. The gelatin backbone of G-PG was able to undergo a sol-gel transition at 4 °C [66], allowing for the formation of a physically crosslinked semi-transparent gel which could also undergo ionic crosslinking and opacify in the presence of $CaCl_2$ (Fig. 7C). Unlike unmodified gelatin, ionically crosslinked G-PG gels were stable after 1 h of incubation at 37 °C (data not shown), indicating that the gel-sol transition of protein backbone was prevented by the ionic crosslinking of PG chains. Tyramine moieties on G-TA-PG allowed for enzymatic crosslinking of 5% w/v solutions into elastic gels with a similar water content (~93.5%) with the 8% SF-PG gels (~93%) (Fig. S3) as well as low hysteresis in the stress-strain curve (Figs. S5A–i) and a compressive modulus of ~2.2 kPa (Fig. S5B). Like SF-PG gels, hysteresis (Figs. S5A–i) and compressive modulus (~10 kPa) increased significantly upon ionic crosslinking in $CaCl_2$ solution and dropped back to initial values after treatment with sodium citrate. Similar hysteresis (Figure S5A-ii) and modulus (Fig. S5B) changes were also recorded for G-TA-PG/SF-PG (1:1) composite gels. Both G-TA-PG and G-TA-PG/SF-PG gels supported cell attachment and survival 24 h after seeding (Fig. S6), confirming that the hydrogel formulations could be utilized for the culture of mammalian cells on mechanically dynamic scaffolds for the investigation of cellular responses.

SEM micrographs of the surface and the cross-sections of the enzymatically crosslinked hydrogels (Fig. S7A) revealed a porous structure for all samples. Unlike 8% SF-PG and 5% G-TA-PG gels which had a porous surface, 3% SF-PG/0.5% G-TA gels displayed a relatively smooth surface morphology. Moreover, 3% SF-PG/0.5% G-TA composite hydrogels had pores with elongated shapes (Fig. S7A) and smaller size (lateral and vertical) (Fig. S7B) than the other samples despite having the lowest total polymer composition. These observations could be explained with the collapse of the 3% SF-PG/0.5% G-TA hydrogel onto itself during lyophilization likely because of lower polymer to water ratio (~0.05) compared to 8% SF-PG or 5% G-TA-PG gels (~0.08) (Fig. S3). It should also be noted that the surface and cross-sectional morphology of the hydrogels may not reflect their native hydrated states due to the potential conformational changes in silk structure during freezing and water removal.

4. Conclusions

Poly(guluronate)-conjugated silk and gelatin hybrid biopolymers were synthesized to combine unique properties of alginate and silk or gelatin for the fabrication of dual crosslinked, mechanically dynamic hydrogel scaffolds. The novel SF-PG constructs reported in the present study not only introduce ionic crosslinking to silk and eliminated potential phase separation issues experienced with silk/alginate blends, but also increased the water solubility of lyophilized silk powders, enabling dry storage for significantly increased shelf-life. Dual crosslinked SF-PG and SF-PG/G-TA gels overperformed ionically or covalently crosslinked alginate-only gels in terms of structural stability in physiological buffers and proteolytic degradation for scaffold remodeling, respectively. Dynamic mechanics through on-demand stiffening by calcium treatment and softening by citrate treatment can enable the modulation of cellular response and fate such as stem cell differentiation, fibrotic response or cancer progression for potential future studies involving a better understanding of biological processes and disease modeling. Successful modification of silk and gelatin with PG chains supports the versatility of the strategy for the synthesis of different protein-PG hybrids for case-specific properties.

Declaration of competing interest

The authors declare that they have no known competing financial interests or personal relationships that could have appeared to influence the work reported in this paper.

Data availability

Data will be made available on request.

Acknowledgements

The authors acknowledge the NSF (2104294, DMR 2104294), the NIH (P41EB027062), the U.S. Air Force (FA9550-17-1-0333 FA8650-15-D-5405) and the ARO (W911NF2120130) for support of this work. We thank Wendy Gavin of University of Massachusetts Core Research Facilities for the GPC analysis of poly(guluronate) samples.

Appendix A. Supplementary data

Supplementary data to this article can be found online at https://doi.org/10.1016/j.polymer.2023.126129.

References

[1] Y.S. Zhang, A. Khademhosseini, Advances in engineering hydrogels, Science 356 (6337) (2017), eaaf3627.
[2] S.R. Caliari, J.A. Burdick, A practical guide to hydrogels for cell culture, Nat. Methods 13 (5) (2016) 405–414.
[3] A. Murua, A. Portero, G. Orive, R.M. Hernández, M. de Castro, J.L. Pedraz, Cell microencapsulation technology: towards clinical application, J. Contr. Release 132 (2) (2008) 76–83.
[4] G. Karoubi, M.L. Ormiston, D.J. Stewart, D.W. Courtman, Single-cell hydrogel encapsulation for enhanced survival of human marrow stromal cells, Biomaterials 30 (29) (2009) 5445–5455.
[5] O. Hasturk, D.L. Kaplan, Cell armor for protection against environmental stress: advances, challenges and applications in micro-and nanoencapsulation of mammalian cells, Acta Biomater. 95 (2019) 3–31.
[6] Z. Sun, C. Song, C. Wang, Y. Hu, J. Wu, Hydrogel-based controlled drug delivery for cancer treatment: a review, Mol. Pharm. 17 (2) (2019) 373–391.
[7] J.C. Garbern, E. Minami, P.S. Stayton, C.E. Murry, Delivery of basic fibroblast growth factor with a pH-responsive, injectable hydrogel to improve angiogenesis in infarcted myocardium, Biomaterials 32 (9) (2011) 2407–2416.
[8] T.D. Johnson, K.L. Christman, Injectable hydrogel therapies and their delivery strategies for treating myocardial infarction, Expet Opin. Drug Deliv. 10 (1) (2013) 59–72.
[9] D. Sivaraj, K. Chen, A. Chattopadhyay, D. Henn, W. Wu, C. Noishiki, N.J. Magbual, S. Mittal, A.M. Mermin-Bunnell, C.A. Bonham, Hydrogel scaffolds to deliver cell therapies for wound healing, Front. Bioeng. Biotechnol. 9 (2021), 660145.
[10] J.A. Burdick, W.L. Murphy, Moving from static to dynamic complexity in hydrogel design, Nat. Commun. 3 (1) (2012) 1269.
[11] Y. Ma, T. Han, Q. Yang, J. Wang, B. Feng, Y. Jia, Z. Wei, F. Xu, Viscoelastic cell microenvironment: hydrogel-based strategy for recapitulating dynamic ECM mechanics, Adv. Funct. Mater. 31 (24) (2021), 2100848.
[12] U. Blache, E.M. Ford, B. Ha, L. Rijns, O. Chaudhuri, P.Y. Dankers, A.M. Kloxin, J. G. Snedeker, E. Gentleman, Engineered hydrogels for mechanobiology, Nature Reviews Methods Primers 2 (1) (2022) 98.

[13] M. Guvendiren, J.A. Burdick, Stiffening hydrogels to probe short-and long-term cellular responses to dynamic mechanics, Nat. Commun. 3 (1) (2012) 792.
[14] L. Teng, Y. Chen, Y.-G. Jia, L. Ren, Supramolecular and dynamic covalent hydrogel scaffolds: from gelation chemistry to enhanced cell retention and cartilage regeneration, J. Mater. Chem. B 7 (43) (2019) 6705–6736.
[15] S.R. Caliari, M. Perepelyuk, E.M. Soulas, G.Y. Lee, R.G. Wells, J.A. Burdick, Gradually softening hydrogels for modeling hepatic stellate cell behavior during fibrosis regression, Integr. Biol. 8 (6) (2016) 720–728.
[16] D.L. Matera, W.Y. Wang, B.M. Baker, New directions and dimensions for bioengineered models of fibrosis, Nat. Rev. Mater. 6 (3) (2021) 192–195.
[17] K. Homma, A.C. Chang, S. Yamamoto, R. Tamate, T. Ueki, J. Nakanishi, Design of azobenzene-bearing hydrogel with photoswitchable mechanics driven by photo-induced phase transition for in vitro disease modeling, Acta Biomater. 132 (2021) 103–113.
[18] Y. Shou, X.Y. Teo, X. Li, L. Zhicheng, L. Liu, X. Sun, W. Jonhson, J. Ding, C.T. Lim, A. Tay, Dynamic magneto-softening of 3D hydrogel reverses malignant transformation of cancer cells and enhances drug efficacy, ACS Nano (2023).
[19] C.M. Madl, L.M. Katz, S.C. Heilshorn, Bio-orthogonally crosslinked, engineered protein hydrogels with tunable mechanics and biochemistry for cell encapsulation, Adv. Funct. Mater. 26 (21) (2016) 3612–3620.
[20] Q. Zhang, Y. Liu, G. Yang, H. Kong, L. Guo, G. Wei, Recent advances in protein hydrogels: from design, structural and functional regulations to healthcare applications, Chem. Eng. J. (2022), 138494.
[21] Q. Yang, J. Peng, H. Xiao, X. Xu, Z. Qian, Polysaccharide hydrogels: functionalization, construction and served as scaffold for tissue engineering, Carbohydrate Polym. 278 (2022), 118952.
[22] J. Sun, H. Tan, Alginate-based biomaterials for regenerative medicine applications, Materials 6 (4) (2013) 1285–1309.
[23] A.D. Augst, H.J. Kong, D.J. Mooney, Alginate hydrogels as biomaterials, Macromol. Biosci. 6 (8) (2006) 623–633.
[24] A.M. Smith, J.J. Senior, Alginate hydrogels with tuneable properties, Tunable Hydrogels: Smart Materials for Biomedical Applications (2021) 37–61.
[25] K.Y. Lee, J.A. Rowley, P. Eiselt, E.M. Moy, K.H. Bouhadir, D.J. Mooney, Controlling mechanical and swelling properties of alginate hydrogels independently by cross-linker type and cross-linking density, Macromolecules 33 (11) (2000) 4291–4294.
[26] I. Sandvig, K. Karstensen, A.M. Rokstad, F.L. Aachmann, K. Formo, A. Sandvig, G. Skjåk-Bræk, B.L. Strand, RGD-peptide modified alginate by a chemoenzymatic strategy for tissue engineering applications, J. Biomed. Mater. Res. 103 (3) (2015) 896–906.
[27] S. Sakai, K. Kawakami, Synthesis and characterization of both ionically and enzymatically cross-linkable alginate, Acta Biomater. 3 (4) (2007) 495–501.
[28] O. Jeon, K.H. Bouhadir, J.M. Mansour, E. Alsberg, Photocrosslinked alginate hydrogels with tunable biodegradation rates and mechanical properties, Biomaterials 30 (14) (2009) 2724–2734.
[29] J.E. Samorezov, C.M. Morlock, E. Alsberg, Dual ionic and photo-crosslinked alginate hydrogels for micropatterned spatial control of material properties and cell behavior, Bioconjugate Chem. 26 (7) (2015) 1339–1347.
[30] R.S. Stilhano, J.L. Madrigal, K. Wong, P.A. Williams, P.K. Martin, F.S. Yamaguchi, V.Y. Samoto, S.W. Han, E.A. Silva, Injectable alginate hydrogel for enhanced spatiotemporal control of lentivector delivery in murine skeletal muscle, J. Contr. Release 237 (2016) 42–49.
[31] R. Londono, S.F. Badylak, Biologic scaffolds for regenerative medicine: mechanisms of in vivo remodeling, Ann. Biomed. Eng. 43 (2015) 577–592.
[32] M.B. Łabowska, K. Cierluk, A.M. Jankowska, J. Kulbacka, J. Detyna, I. Michalak, A review on the adaption of alginate-gelatin hydrogels for 3D cultures and bioprinting, Materials 14 (4) (2021) 858.
[33] K. Chen, S. Vyazovkin, Temperature dependence of sol-gel conversion kinetics in gelatin-water system, Macromol. Biosci. 9 (4) (2009) 383–392.
[34] R. Silva, R. Singh, B. Sarker, D.G. Papageorgiou, J.A. Juhasz, J.A. Roether, I. Cicha, J. Kaschta, D.W. Schubert, K. Chrissafis, Soft-matrices based on silk fibroin and alginate for tissue engineering, Int. J. Biol. Macromol. 93 (2016) 1420–1431.
[35] C. Vepari, D.L. Kaplan, Silk as a biomaterial, Prog. Polym. Sci. 32 (8–9) (2007) 991–1007.
[36] H. Li, N. Li, H. Zhang, Y. Zhang, H. Suo, L. Wang, M. Xu, Three-dimensional bioprinting of perfusable hierarchical microchannels with alginate and silk fibroin double cross-linked network, 3D Print. Addit. Manuf. 7 (2) (2020) 78–84.
[37] B.P. Partlow, C.W. Hanna, J. Rnjak-Kovacina, J.E. Moreau, M.B. Applegate, K. A. Burke, B. Marelli, A.N. Mitropoulos, F.G. Omenetto, D.L. Kaplan, Highly tunable elastomeric silk biomaterials, Adv. Funct. Mater. 24 (29) (2014) 4615–4624.
[38] S. Choi, H. Ahn, S.H. Kim, Tyrosinase-mediated hydrogel crosslinking for tissue engineering, J. Appl. Polym. Sci. 139 (14) (2022), 51887.
[39] J. Choi, M. McGill, N.R. Raia, O. Hasturk, D.L. Kaplan, Silk hydrogels crosslinked by the fenton reaction, Adv Healthc Mater 8 (17) (2019), 1900644.
[40] M.B. Applegate, B.P. Partlow, J. Coburn, B. Marelli, C. Pirie, R. Pineda, D. L. Kaplan, F.G. Omenetto, Photocrosslinking of silk fibroin using riboflavin for ocular prostheses, Adv. Mater. 28 (12) (2016) 2417–2420.
[41] L.M. Lopes, M.A. De Moraes, M.M. Beppu, Phase diagram and estimation of flory-huggins parameter of interaction of silk fibroin/sodium alginate blends, Front. Bioeng. Biotechnol. 8 (2020) 973.
[42] K.H. Bouhadir, D.S. Hausman, D.J. Mooney, Synthesis of cross-linked poly (aldehyde guluronate) hydrogels, Polymer 40 (12) (1999) 3575–3584.
[43] H.M. Lee, Y.-H. Yoon, W.-B. Lee, J.-K. Kim, A gel-forming poly-l-guluronic acid produced from no guluronate-rich marine algae using new hydrolysis method: test for endovascular embolization, J. Mater. Sci. Mater. Med. 20 (2009) 1917–1926.
[44] O. Hasturk, J.A. Smiley, M. Arnett, J.K. Sahoo, C. Staii, D.L. Kaplan, Cytoprotection of human progenitor and stem cells through encapsulation in alginate templated, dual crosslinked silk and silk-gelatin composite hydrogel microbeads, Adv Healthc Mater 11 (17) (2022). ARTN 220029310.1002/adhm.202200293. PubMed PMID: WOS:000814182900001.
[45] A.R. Murphy, D.L. Kaplan, Biomedical applications of chemically-modified silk fibroin, J. Mater. Chem. 19 (36) (2009) 6443–6450.
[46] O. Hasturk, J.K. Sahoo, D.L. Kaplan, Synthesis and characterization of silk ionomers for layer-by-layer electrostatic deposition on individual mammalian cells, Biomacromolecules 21 (7) (2020) 2829–2843, https://doi.org/10.1021/acs.biomac.0c00523. PubMed PMID: WOS:000599012600025.
[47] Z. Zhang, G. Yu, X. Zhao, H. Liu, H. Guan, A.M. Lawson, W. Chai, Sequence analysis of alginate-derived oligosaccharides by negative-ion electrospray tandem mass spectrometry, J. Am. Soc. Mass Spectrom. 17 (2006) 621–630.
[48] C.Z. Zhou, F. Confalonieri, M. Jacquet, R. Perasso, Z.G. Li, J. Janin, Silk fibroin: structural implications of a remarkable amino acid sequence, Proteins: Struct., Funct., Bioinf. 44 (2) (2001) 119–122.
[49] K. Nultsch, L.K. Bast, M. Näf, S.E. Yakhlifi, N. Bruns, O. Germershaus, Effects of silk degumming process on physicochemical, tensile, and optical properties of regenerated silk fibroin, Macromol. Mater. Eng. 303 (12) (2018), 1800408.
[50] Y. Tamada, New process to form a silk fibroin porous 3-D structure, Biomacromolecules 6 (6) (2005) 3100–3106.
[51] F. Lin, Y. Li, J. Jin, Y. Cai, K. Wei, J. Yao, Deposition behavior and properties of silk fibroin scaffolds soaked in simulated body fluid, Mater. Chem. Phys. 111 (1) (2008) 92–97.
[52] J.K. Sahoo, J. Choi, O. Hasturk, I. Laubach, M.L. Descoteaux, S. Mosurkal, B. Wang, N. Zhang, D.L. Kaplan, Silk degumming time controls horseradish peroxidase-catalyzed hydrogel properties, Biomater Sci-Uk 8 (15) (2020) 4176–4185.
[53] J.A. Kluge, B.T. Kahn, J.E. Brown, F.G. Omenetto, D.L. Kaplan, Optimizing molecular weight of lyophilized silk as a shelf-stable source material, ACS Biomater. Sci. Eng. 2 (4) (2016) 595–605.
[54] N. Cao, X. Chen, D. Schreyer, Influence of calcium ions on cell survival and proliferation in the context of an alginate hydrogel, Int. Sch. Res. Notices 2012 (2012).
[55] L. Li, Y. Chen, Y. Wang, F. Shi, Y. Nie, T. Liu, K. Song, Effects of concentration variation on the physical properties of alginate-based substrates and cell behavior in culture, Int. J. Biol. Macromol. 128 (2019) 184–195.
[56] S. Haeberle, L. Naegele, R. Burger, Stetten Fv, R. Zengerle, J. Ducree, Alginate bead fabrication and encapsulation of living cells under centrifugally induced artificial gravity conditions, J. Microencapsul. 25 (4) (2008) 267–274.
[57] O. Hasturk, K.E. Jordan, J. Choi, D.L. Kaplan, Enzymatically Crosslinked Silk and Silk-Gelatin Hydrogels with Tunable Gelation Kinetics, Mechanical Properties and Bioactivity for Cell Culture and Encapsulation, Biomaterials, 2020, p. 232. ARTN 119720 10.1016/j.biomaterials.2019.119720. PubMed PMID: WOS:000514748200013.
[58] K.Y. Lee, D.J. Mooney, Alginate: properties and biomedical applications, Prog. Polym. Sci. 37 (1) (2012) 106–126.
[59] I. Machida-Sano, M. Hirakawa, H. Matsumoto, M. Kamada, S. Ogawa, N. Satoh, H. Namiki, Surface characteristics determining the cell compatibility of ionically cross-linked alginate gels, Biomed. Mater. 9 (2) (2014), 025007.
[60] K. Su, C. Wang, Recent advances in the use of gelatin in biomedical research, Biotechnol. Lett. 37 (2015) 2139–2145.
[61] Y. Li, J. Rodrigues, H. Tomas, Injectable and biodegradable hydrogels: gelation, biodegradation and biomedical applications, Chem. Soc. Rev. 41 (6) (2012) 2193–2221.
[62] B. Zhu, H. Yin, Alginate lyase: review of major sources and classification, properties, structure-function analysis and applications, Bioengineered 6 (3) (2015) 125–131.
[63] Q. Lu, B. Zhang, M. Li, B. Zuo, D.L. Kaplan, Y. Huang, H. Zhu, Degradation mechanism and control of silk fibroin, Biomacromolecules 12 (4) (2011) 1080–1086.
[64] R. Hafidz, C. Yaakob, I. Amin, A. Noorfaizan, Chemical and functional properties of bovine and porcine skin gelatin, Int. Food Res. J. 18 (2) (2011) 787–791.
[65] Y.P. Lim, A.W. Mohammad, Physicochemical properties of mammalian gelatin in relation to membrane process requirement, Food Bioprocess Technol. 4 (2011) 304–311.
[66] PJdA. Sobral, A. Habitante, Phase transitions of pigskin gelatin, Food Hydrocolloids 15 (4–6) (2001) 377–382.